THE JOURNAL OF BIOLOGICAL CHEMISTRY VOL. 291, NO. 22, pp. 11529–11539, May 27, 2016


# Fine-tuning of Substrate Affinity Leads to Alternative Roles of *Mycobacterium tuberculosis* $Fe^{2+}$-ATPases*

Received for publication, January 29, 2016, and in revised form, March 24, 2016 Published, JBC Papers in Press, March 28, 2016, DOI 10.1074/jbc.M116.718239

**Sarju J. Patel[‡], Brianne E. Lewis[§], Jarukit E. Long[¶], Subhalaxmi Nambi[¶], Christopher M. Sassetti[¶‖], Timothy L. Stemmler[§], and José M. Argüello[‡1]**

*From the [‡]Department of Chemistry and Biochemistry, Worcester Polytechnic Institute, Worcester, Massachusetts 01609, [§]Department of Pharmaceutical Sciences, Wayne State University, Detroit, Michigan 48201, [¶]Department of Microbiology and Physiological Systems, University of Massachusetts Medical School, Worcester, Massachusetts 01655, and [‖]Howard Hughes Medical Institute, Chevy Chase, Maryland 20815*

**Little is known about iron efflux transporters within bacterial systems. Recently, the participation of *Bacillus subtilis* PfeT, a $P_{1B4}$-ATPase, in cytoplasmic $Fe^{2+}$ efflux has been proposed. We report here the distinct roles of mycobacterial $P_{1B4}$-ATPases in the homeostasis of $Co^{2+}$ and $Fe^{2+}$. Mutation of *Mycobacterium smegmatis ctpJ* affects the homeostasis of both ions. Alternatively, an *M. tuberculosis ctpJ* mutant is more sensitive to $Co^{2+}$ than $Fe^{2+}$, whereas mutation of the homologous *M. tuberculosis ctpD* leads to $Fe^{2+}$ sensitivity but no alterations in $Co^{2+}$ homeostasis. *In vitro*, the three enzymes are activated by both $Fe^{2+}$ and $Co^{2+}$ and bind 1 eq of either ion at their transport site. However, equilibrium binding affinities and activity kinetics show that *M. tuberculosis* CtpD has higher affinity for $Fe^{2+}$ and twice the $Fe^{2+}$-stimulated activity than the CtpJs. These parameters are paralleled by a lower activation and affinity for $Co^{2+}$. Analysis of $Fe^{2+}$ and $Co^{2+}$ binding to CtpD by x-ray absorption spectroscopy shows that both ions are five- to six-coordinate, constrained within oxygen/nitrogen environments with similar geometries. Mutagenesis studies suggest the involvement of invariant Ser, His, and Glu residues in metal coordination. Interestingly, replacement of the conserved Cys at the metal binding pocket leads to a large reduction in $Fe^{2+}$ but not $Co^{2+}$ binding affinity. We propose that CtpJ ATPases participate in the control of steady state $Fe^{2+}$ levels. CtpD, required for *M. tuberculosis* virulence, is a high affinity $Fe^{2+}$ transporter involved in the rapid response to iron dyshomeostasis generated upon redox stress.**

Iron is an essential micronutrient required for numerous biological processes as it is used as a prosthetic group by several different enzymes (1, 2). However, in excess, it can be toxic due to its participation in Fenton chemistry and potential mismetallation in non-iron-containing metalloproteins. In this context, damage of iron-sulfur centers and mononuclear iron enzymes produced by various redox stresses are particular contributors to iron dyshomeostasis and consequent toxicity (3–6). Characterization of bacterial $Fe^{2+}$ homeostasis has mainly been focused in mechanisms of uptake (by divalent metal, siderophore, and heme transporters), transcriptional regulation (by Fur and IdeR systems), and $Fe^{2+}$ sequestration (by bacterioferritin and Dps proteins) (2, 7–9). Nevertheless, studies have suggested that cation diffusion facilitators and iron-citrate transporters participate in $Fe^{2+}$ efflux (10–12). We recently observed that *Bacillus subtilis* PfeT, a $P_{1B4}$-ATPase, confers $Fe^{2+}$ tolerance (13). PfeT is expressed under the control of PerR in response to peroxide exposure (14). Initial biochemical characterization showed that $Fe^{2+}$ activates isolated PfeT ATPase, leading to a higher $V_{max}$ than generated by $Co^{2+}$, which is the proposed substrate of $P_{1B4}$-ATPases (13, 15–17). Interestingly, phenotypic analysis of *Listeria monocytogenes* lacking the $P_{1B4}$-ATPase FrvA showed a role of this ATPase in resistance to heme toxicity (18). These observations suggest a significant role of this subfamily of P-type ATPases in $Fe^{2+}$ homeostasis (13, 14).

$P_{1B4}$-ATPases present in prokaryotes and plant chloroplasts are part of the large family of P-type ATPases (15, 19, 20). P-type ATPases are polytopic membrane proteins that transport a variety of ions using the energy provided by ATP hydrolysis (21–23). The $P_{1B}$ subgroup includes proteins responsible for the efflux of cytoplasmic transition metals including $Cu^{+}$, $Zn^{2+}$, $Co^{2+}$, and $Ni^{2+}$ (19, 22, 23). The specificity of their transmembrane metal binding sites (TM-MBSs)[2] is determined by invariant amino acid sequences in their last three transmembrane segments (TMs) (17, 19, 24–26). However, activation by non-cognate substrates has been reported for most $P_{1B}$-ATPase subgroups (22, 27). In particular, activation of $P_{1B4}$-ATPases by $Co^{2+}$, $Ni^{2+}$, $Ca^{2+}$, $Cu^{+}$, $Zn^{2+}$, and $Cd^{2+}$ has been proposed (15–17, 28–30). We previously reported *in vivo* and *in vitro* functional studies directed at understanding the metal selectivity and consequent physiological roles of mycobacterial $P_{1B4}$-ATPases (15, 16). The presence of one or two $P_{1B4}$-ATPase-coding genes in mycobacterial species enabled comparative studies of *Mycobacterium smegmatis* CtpJ and *Mycobacterium*

* This work was supported by National Institutes of Health Grant DK068139 (to T. L. S.). The authors declare that they have no conflicts of interest with the contents of this article. The content is solely the responsibility of the authors and does not necessarily represent the official views of the National Institutes of Health.

[1] To whom correspondence should be addressed: Dept. of Chemistry and Biochemistry, Worcester Polytechnic Institute, 100 Institute Rd., Worcester, MA 01609. Tel.: 508-831-5326; Fax: 508-831-4116; E-mail: arguello@wpi.edu.

[2] The abbreviations used are: TM-MBS, transmembrane metal binding site; AAS, atomic absorbance spectroscopy; EXAFS, extended x-ray absorption fine structure; LIMM, low iron defined medium; STN, streptonigrin; TM, transmembrane segment; XANES, x-ray absorption near edge spectroscopy; XAS, x-ray absorption spectroscopy; Ms, *M. smegmatis*; Mt, *M. tuberculosis*; TCEP, tris(2-carboxyethyl)phosphine.

*tuberculosis* CtpJ and CtpD. *In vitro*, MsCtpJ and MtCtpJ display a higher activation by $Co^{2+}$ and $Ni^{2+}$ compared with $Zn^{2+}$, although equilibrium binding affinities show $K_D$ values for $Zn^{2+} < Co^{2+} = Ni^{2+}$ (15, 16). *In vivo*, *ctpJ* expression is induced by $Co^{2+}$, whereas mutant strains show accumulation and sensitivity to the metal. On the contrary, the expression of the homologous *MtctpD* is not induced by $Co^{2+}$ but rather by redox stress. Mutation of *MtctpD* does not lead to $Co^{2+}$ sensitivity or higher intracellular levels of this metal. Nevertheless, MtCtpD ATPase activity is partially activated by $Co^{2+}$. Surprisingly, MtCtpD but not MtCtpJ is required for *M. tuberculosis* virulence.

Previous studies have not explored the activation of mycobacterial $P_{1B4}$-ATPases by $Fe^{2+}$. Could a differential activation by $Co^{2+}/Fe^{2+}$ explain the presence of paralogous genes in *M. tuberculosis*? Why is MtCtpD but not MtCtpJ required for virulence? To address these questions, we examined the activation of *M. smegmatis* and *M. tuberculosis* $P_{1B4}$-ATPases by $Fe^{2+}$ and their participation in $Fe^{2+}$ homeostasis and stress response. In addition, we explored the molecular basis of the different $Fe^{2+}$ and $Co^{2+}$-ATPase activities by determining the coordination of these metals during transport by MtCtpD.

## Experimental Procedures

*Mycobacterium Strains and Culture Conditions—M. smegmatis* mc2155, *M. tuberculosis* H37Rv, and derived strains were grown in 7H9 liquid medium (BD Biosciences, Difco) supplemented with 0.2% glycerol, 0.05% Tween 80, and 10% ADN supplement (0.5% bovine serum albumin, 0.2% dextrose, and 0.085% NaCl) or in low iron defined medium (LIMM) containing 0.5% L-asparagine, 0.5% $KH_2PO_4$, 2% glycerol, 0.05% Tween 80, and 10% ADN, pH 6.8 (31). LIMM was treated with Chelex-100 (Sigma) and before use supplemented with 3.7 $\mu$M $ZnCl_2$, 0.8 $\mu$M $MnCl_2$, and 0.4 mM $MgCl_2$. This medium contained less than 1 $\mu$M residual iron as determined by atomic absorption spectroscopy (AAS) (PerkinElmer Life Sciences PinAAcle 900z). Construction of *Ms*Δ*ctpJ* (MSMEG_5403), *Mt*Δ*ctpD* (Rv1469), *Mt*Δ*ctpJ* (Rv3743), and *Mt*Δ*ctpD*:Δ*ctpJ* mutant and complemented strains was described previously (15, 16).

*Iron and Hemin Sensitivity Tests*—Liquid LIMM cultures of *M. smegmatis* mc2155, *M. tuberculosis* H37Rv, mutant, and complemented strains were inoculated at 0.05 $A_{600}$ from late exponential phase cultures and supplemented with the desired concentration of $FeCl_3$ or hemin (Sigma). A hemin stock solution was prepared at 25 mg/ml in 1.4 M NaOH. Cells were incubated for 16 h (*M. smegmatis*) or 5 days (*M. tuberculosis*), and $A_{600}$ was measured. To avoid hemin interference in $A_{600}$ readings, cells grown in hemin-containing medium were collected, washed twice with LIMM, and suspended in the original LIMM volume, and $A_{600}$ was measured.

*Streptonigrin Sensitivity Tests—M. smegmatis* mc2155, *M. tuberculosis* H37Rv, mutant, and complemented strains grown in LIMM to midlog phase were diluted to 0.05 $A_{600}$ in LIMM. The cultures were supplemented with 1 $\mu$g ml$^{-1}$ streptonigrin (STN) and 10 $\mu$M $FeCl_3$ as indicated in the figures. Cells were incubated for 16 h (*M. smegmatis*) or 5 days (*M. tuberculosis*), and $A_{600}$ was measured.

*Metal Accumulation Assays*—Liquid LIMM cultures in mid-exponential phase ($A_{600} \sim 1.0$) were supplemented with increasing concentrations of $FeCl_3$ and incubated for 4 (*M. smegmatis*) or 8 h (*M. tuberculosis*). After this incubation, cells were harvested and washed with 5 mM EDTA and 0.9% NaCl. Aliquots were taken for protein determinations (32). Pellets were acid-digested with 0.5 ml of $NO_3H$ for 1 h at 80 °C and then overnight at 20 °C. Digestions were concluded by adding ⅛ volume of 30% (v/v) $H_2O_2$ followed by a 1:5 dilution with water. Metal contents in digested samples were measured by AAS.

*Protein Expression and Purification*—Preparation of *E. coli* LMG194 Δ*copA* strains carrying *M. smegmatis ctpJ* (MSMEG_5403) or *M. tuberculosis ctpD* (Rv1469) or *ctpJ* (Rv3743) in pBAD-TOPO/His vectors was described previously (15, 16). Cells were grown at 37 °C in ZYP-505 autoinduction medium supplemented with 0.05% arabinose, 100 mg ml$^{-1}$ ampicillin, and 50 mg ml$^{-1}$ kanamycin (33). Cells were harvested at 16 h postinoculation; washed with 25 mM Tris, pH 7.0, 100 mM KCl, and 20% glycerol; and stored at −70 °C. Expressed mycobacterial proteins contained a C-terminal $His_6$ tag sequence preceded by a tobacco etch virus protease recognition sequence. Protein purification was carried out as described previously (15, 24, 34). Briefly, cells were disrupted in a French press, and membranes were isolated by centrifugation. Membranes were treated with 0.75% dodecyl β-D-maltoside (Calbiochem), 25 mM Tris, pH 8.0, 100 mM sucrose, 500 mM NaCl, and 1 mM phenylmethylsulfonyl fluoride. The solubilized membrane protein suspension was cleared by centrifugation at 163,000 × *g* for 1 h, and proteins were affinity-purified using $Ni^{2+}$-nitrilotriacetic acid resin. The $His_6$ tag was removed from the C terminus by treatment with $His_6$-tagged tobacco etch virus protease (35). Tobacco etch virus-$His_6$ was removed by affinity purification with $Ni^{2+}$-nitrilotriacetic acid resin. Protein purity was analyzed by 10% SDS-PAGE followed by Coomassie Brilliant Blue staining or Western blotting using an anti-$His_6$ tag antibody (GenScript, Piscataway, NJ). Isolated proteins (3 mg/ml) were stored at −20 °C in 25 mM Tris, pH 8.0, 100 mM sucrose, 50 mM NaCl, 0.01% dodecyl β-D-maltoside, 0.01% asolectin, 1 mM phenylmethylsulfonyl fluoride, and 20% glycerol. Prior to ATPase activity determinations, proteins (1 mg/ml) were treated with 0.5 mM EDTA and 0.5 mM tetrathiomolybdate for 45 min at room temperature. Chelators were removed using Ultra-30 Centricon (Millipore, Darmstadt, Germany) filtration devices.

*Mutagenesis of MtCtpD Metal Binding Site—MtctpD* cloned into pBAD-TOPO/His vector was used as a template to introduce the mutations coding for the single substitutions Ser-316 (S316A), Cys-318 (C318A), His-642 (H642A), Glu-643 (E643A and E643D), Gly-644 (G644A), Ser-645 (S645A), and Thr-646 (T646A and T646S) and the multiple replacements S316C/C318S. All mutations were introduced using a Q5® site-directed mutagenesis kit (New England Biolabs, Ipswich, MA). The sequences of primers used in this study are available upon request to the corresponding author. DNA sequences were confirmed by automated sequencing.

*$Fe^{2+}$ Binding to Proteins*—Metal binding to isolated enzymes was measured as described previously (15, 36). Five micromolar His-less enzyme was incubated for 1 min at 4 °C in 25 mM HEPES-NaOH, pH 7.5, 150 mM NaCl, 1 mM tris(2-carboxyethyl)phosphine (TCEP), and 20 $\mu$M either $FeSO_4$ or $CoCl_2$. Excess metal was removed by washing in a 30-kDa-cutoff Centricon filtration device. Protein samples were acid-digested as described above, and metal concentrations were measured using AAS.

Metal binding affinities were determined using the divalent metal-binding chromophore mag-fura-2 (Invitrogen) (15, 36). Five micromolar His-less protein and 10 $\mu$M mag-fura-2 were titrated with 1 mM $Fe^{2+}$ or $Co^{2+}$ in Chelex-treated buffer (25 mM HEPES-NaOH, pH 7.5, 150 mM NaCl, and 1 mM TCEP). Free mag-fura-2 was determined by monitoring $A_{366}$ ($\epsilon_{366}$ 29,900 1/M·cm). Free metal concentrations were calculated from $K_I = [I{\cdot}Me^{2+}]/[I_{free}][Me^{2+}{}_{free}]$ where $I$ is mag-fura-2, Me is the metal ion, and $K_I$ is the association constant of mag-fura-2 with each metal. $K_D$ values of 1.5 $\mu$M for $Fe^{2+}$ and 2.8 $\mu$M for $Co^{2+}$ were experimentally determined for the metal/mag-fura-2 interactions. The metal-protein $K_D$ values were calculated from $\nu = n[Me^{2+}{}_{free}]/K_D(1 + ([Me^{2+}{}_{free}]/K_D)$ where $\nu$ is the molar ratio of metal bound to protein and $n$ is the apparent stoichiometry (37). Reported errors for $K_D$ and $n$ are asymptotic standard errors provided by the fitting software KaleidaGraph (Synergy, Reading, PA).

*ATPase Assays*—ATPase assays were performed as described (15, 24, 34). The assay mixture contained 50 mM Tris, pH 7.4, 50 mM NaCl, 3 mM $MgCl_2$, 3 mM ATP, 0.01% asolectin, 0.01% dodecyl $\beta$-D-maltoside, 2.5 mM TCEP, 20 $\mu$g/ml purified protein, and freshly prepared transition metal ions at the desired concentrations. $Fe^{3+}$ was added as $FeCl_3$, $Cu^{2+}$ was added as $CuSO_4$, and in both cases TCEP was not included in the assay medium. $Cu^{+}$ was obtained by including TCEP with $CuSO_4$ salt. $Fe^{2+}$ and $Zn^{2+}$ were included in the assay medium as the sulfate salts, whereas $Co^{2+}$, $Ni^{2+}$, and $Mn^{2+}$ were included as their chloride salts. ATPase activity was stopped after a 20-min incubation at 37 °C, and released $P_i$ was determined (38). ATPase activity measured in the absence of transition metals was subtracted from plotted values. Curves of ATPase activity metal dependence were fit to $\nu = V_{max}[Me^{+/2+}]/([Me^{+/2+}] + K_{1/2})$. The reported standard errors for $V_{max}$ and $K_{1/2}$ are asymptotic standard errors reported by the fitting software KaleidaGraph.

*X-ray Absorption Spectroscopy (XAS)*—XAS samples were loaded in a Coy anaerobic chamber at a 1:1 metal:protein molar ratio (1.2 mM $Fe^{2+}$ or 0.43 mM $Co^{2+}$). Sample was injected into a Kapton-wrapped Lucite cell, flash frozen, and stored in liquid nitrogen. XAS data were collected at the Stanford Synchrotron Radiation Lightsource on beamline 7-3 equipped with a Si(220) double crystal monochromator with a harmonic rejection mirror. Fluorescence spectra were collected using a 30-element germanium solid-state detector (Canberra, Meriden, CT). During data collection, the continuous flow liquid helium cryostat (Oxford Instruments, Concord, MA) was stabilized at 10 K. Iron and cobalt data were collected using a 6-$\mu$m magnesium or a 3-$\mu$m iron filter, respectively, placed between the cryostat and the detector to reduce unassociated scattering. Iron and cobalt foil spectra were collected simultaneously with protein data for direct energy calibration of the data. The first inflection points for iron and cobalt were set at 7111.3 and 7709.5 eV, respectively. Iron XAS spectra were recorded using 5-eV steps in the pre-edge regions (6900–7094 eV), 0.25-eV steps in the edge regions (7095–7135 eV), and 0.05-$Å^{-1}$ increments in the extended x-ray absorption fine structure (EXAFS) region (to $k$ = 13.5 $Å^{-1}$), integrating from 1 to 20 s in a $k^3$-weighted manner. Cobalt XAS spectra were recorded using 5-eV steps in the pre-edge regions (7542–7702 eV), 0.25-eV steps in the edge regions (7702–7780 eV), and 0.05-$Å^{-1}$ increments in the extended EXAFS region (to $k$ = 13.5 $Å^{-1}$), integrating from 1 to 25 s in a $k^3$-weighted manner. A total of eight scans were taken for each sample, and these were then averaged.

XAS spectra were processed and analyzed using the EXAFSPAK program suite for Macintosh OSX (39). A Gaussian function was used in the pre-edge region, and a three-region cubic spline was used in the EXAFS region. EXAFS data were converted to $k$ space using $E_0$ values of 7130 and 7745 eV for iron and cobalt, respectively. Spectra were simulated using single and multiple scattering amplitude and phase functions generated using the Feff v8 software integrated within EXAFSPAK. Single scattering models were calculated for oxygen, nitrogen, and carbon to simulate possible iron- or cobalt-ligand environment. Calibrated scale factors and model $E_0$ values were not allowed to vary during fitting; the scale factor for iron was 0.95, and that for cobalt was 0.98. Iron data were fit out to a $k$ value of 13.5 $Å^{-1}$. Calibration from $Fe^{2+}$ and $Fe^{3+}$ model compounds was used for determination of $E_0$ and scale factor parameters for iron. $E_0$ values for Fe–O and Fe–C were set at −10 eV. Cobalt data were fit out to a $k$ value of 13.5 $Å^{-1}$. Calibration from $Co^{2+}$ model compounds was used for determination of $E_0$ and scale factor parameters. $E_0$ values for Co–O and Co–C were set at −11.3 eV. EXAFS spectra were simulated using both filtered and unfiltered data; however, simulation results are presented only for fits to unfiltered (raw) data. Simulation protocols and criteria for determining the best fit have been described elsewhere (25).

## Results

*Mycobacterial $P_{1B4}$-ATPases Confer $Fe^{2+}$ Tolerance*—We previously reported the activation of mycobacterial $P_{1B4}$-ATPases by $Co^{2+}$ (15, 16). However, *M. tuberculosis* CtpJ and CtpD appear to have distinct roles in $Co^{2+}$ tolerance and cellular response to redox stress (16). We recently observed that *B. subtilis* PfeT, a $P_{1B4}$-ATPase in the PerR regulon, transports and confers tolerance to $Fe^{2+}$ in addition to $Co^{2+}$ (13). Similarly, the *L. monocytogenes* $P_{1B4}$-ATPase, FrvA, confers resistance to heme toxicity (18). Thus, we hypothesized that selective activation by $Fe^{2+}$ might explain the presence of the *ctpJ* and *ctpD* paralogs in the *M. tuberculosis* genome. To test this idea, the capability of mycobacterial $P_{1B4}$-ATPases to confer tolerance to $Fe^{2+}$ was assessed. Fig. 1 shows the growth of *Ms*Δ*ctpJ*, *Mt*Δ*ctpD*, *Mt*Δ*ctpJ*, and *Mt*Δ*ctpD*:Δ*ctpJ* double mutant strains in LIMM supplemented with different concentrations of $FeCl_3$ or hemin. The *Ms*Δ*ctpJ* strain showed a growth defect at high $FeCl_3$ or hemin as compared with

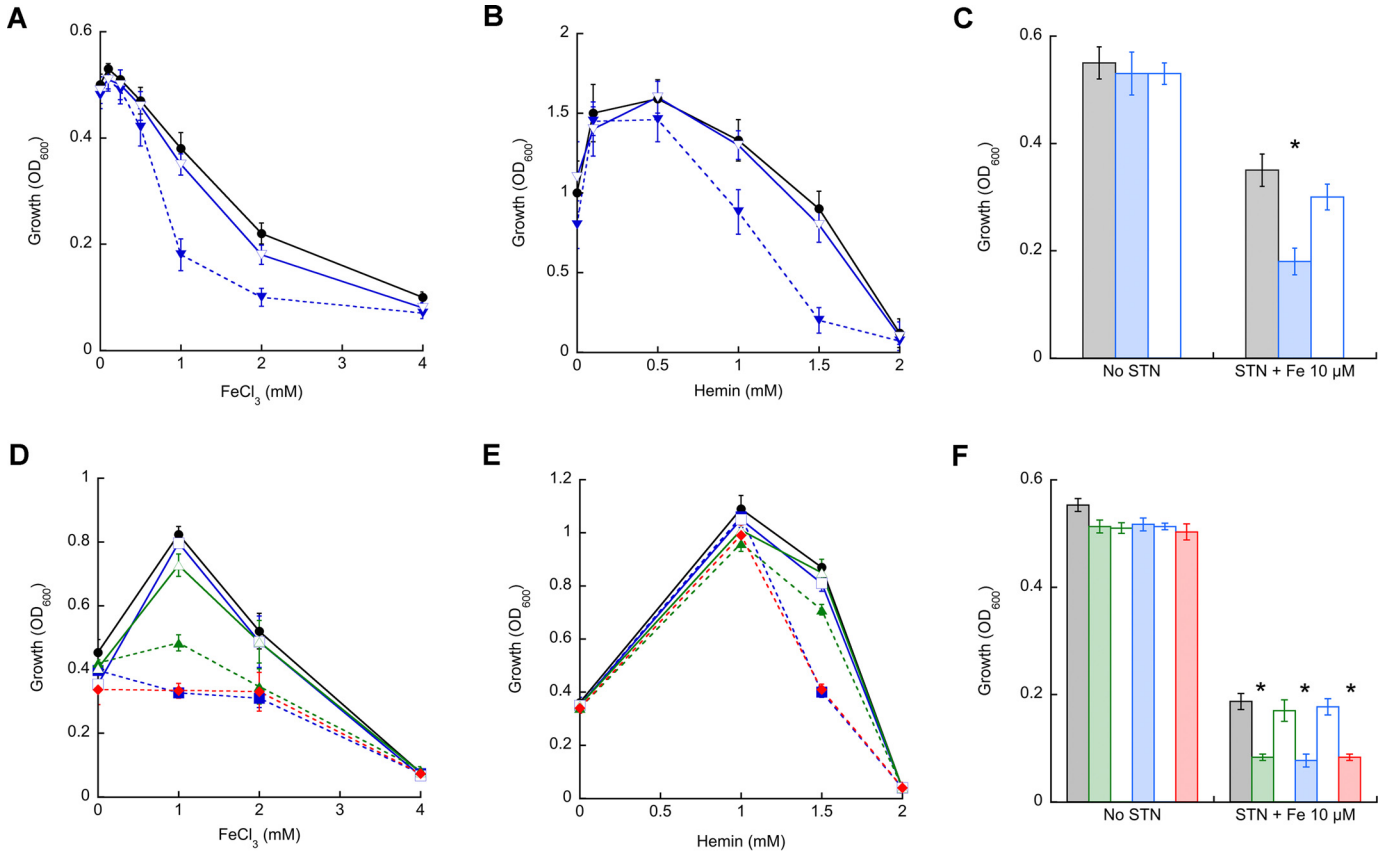


FIGURE 1. **Growth response of mycobacterial $P_{1B4}$-ATPase mutant strains to iron, hemin, and streptonigrin/iron.** *A* and *B*, *M. smegmatis* WT (●; *black*) and Δ*ctpJ* (▼; *blue*) and complemented (▽; *blue*) strains were grown in the presence of increasing concentrations of $FeCl_3$ (*A*) or hemin (*B*) in the LIMM for 16 h, and $A_{600}$ was measured. *C*, *M. smegmatis* WT (*gray bars*), Δ*ctpJ* (*blue bars*), and complemented (*white bars*) strains were grown in LIMM supplemented with 1 μg ml$^{-1}$ STN and 10 μM $FeCl_3$, and growth was measured at 16 h. *D* and *E*, *M. tuberculosis* WT (●; *black*), Δ*ctpD* (■; *blue*) and complemented (□; *blue*), Δ*ctpJ* (▲; *green*) and complemented (△; *green*), and Δ*ctpD*:Δ*ctpJ* (◆; *red*) strains were grown in the presence of increasing concentrations of $FeCl_3$ (*D*) or hemin (*E*) in LIMM for 5 days, and $A_{600}$ was measured. *F*, *M. tuberculosis* WT (*gray bars*), Δ*ctpD* (*green bars*), Δ*ctpD* complemented (*white bars*), Δ*ctpJ* (*blue bars*), Δ*ctpJ* complemented (*white bars*), and Δ*ctpD*:Δ*ctpJ* (*red bars*) strains were grown in LIMM supplemented with 1 μg ml$^{-1}$ STN and 10 μM $FeCl_3$, growth was measured at 5 days, and $A_{600}$ was measured. Data are the mean ± S.E. (*error bars*) of three independent experiments. Significant differences from the WT as determined by Student's *t* test are indicated (*, $p < 0.05$).

*M. smegmatis* WT (Fig. 1, *A* and *B*). The complemented *Ms*Δ*ctpJ* strain, carrying the plasmid pMV306 harboring the full-length *MsctpJ* gene under the regulation of its native promoter, showed similar growth as the *M. smegmatis* WT. A comparable deficiency was observed in the *Mt*Δ*ctpJ* strain grown in the presence of 1 mM $FeCl_3$ (Fig. 1*D*). However, this mutant strain was not affected by the presence of hemin in the medium. On the contrary, mutation of the *MtctpD* gene significantly affected the growth in both $FeCl_3$- and hemin-supplemented medium. Interestingly, the *Mt*Δ*ctpD*:Δ*ctpJ* double mutant strain showed a behavior identical to that of the *Mt*Δ*ctpD* strain. In all cases, complemented strains showed the growth phenotype of *M. tuberculosis* WT (Fig. 1, *D* and *E*). The data indicate that MsCtpJ and MtCtpD confer iron tolerance when cells are exposed to relatively high metal levels. Exploring their role at lower iron levels, the sensitivity to STN was tested. STN is a quinone antibiotic whose activity is correlated with intracellular iron availability (40). The *Ms*Δ*ctpJ*, *Mt*Δ*ctpD*, *Mt*Δ*ctpJ*, and *Mt*Δ*ctpD*:Δ*ctpJ* mutant strains displayed a significantly increased STN sensitivity in LIMM supplemented with 1 μg ml$^{-1}$ STN and only 10 μM $FeCl_3$ (Fig. 1, *C* and *F*). In contrast to their distinct tolerance to high $Fe^{3+}$ in the medium, there was no significant difference in the sensitivity of *Mt*Δ*ctpD* and *Mt*Δ*ctpJ* strains to STN-$Fe^{2+}$.

These results suggest that to different extents mycobacterial $P_{1B4}$-ATPases contribute to $Fe^{2+}$ homeostasis by driving this metal efflux. To further explore this hypothesis, *Ms*Δ*ctpJ*, *Mt*Δ*ctpD*, *Mt*Δ*ctpJ*, and *Mt*Δ*ctpD*:Δ*ctpJ* mutant strains were challenged with sublethal concentrations of $FeCl_3$, and the resulting cellular $Fe^{2+}$ levels were determined. Consistent with the iron sensitivity phenotypes (Fig. 1), $Fe^{2+}$ accumulation was observed in mutant strains (Fig. 2, *A* and *B*). Iron levels in the *Ms*Δ*ctpJ* strain were approximately 5 times higher than those in *M. smegmatis* WT (Fig. 2*A*). The partial recovery observed in the *Ms*Δ*ctpJ* mutant strain complemented with *MsctpJ* appears to be associated with lower levels of transcript (35% of WT; not shown). Reinforcing the predominant role of MtCtpD in $Fe^{2+}$ homeostasis, a significant increase of $Fe^{2+}$ content was observed in the *Mt*Δ*ctpD* strain, whereas 50% smaller changes were observed in the *Mt*Δ*ctpJ* strain. Similar $Fe^{2+}$ accumulation was observed in the *Mt*Δ*ctpD* and *Mt*Δ*ctpD*:Δ*ctpJ* double mutant strains (Fig. 2*B*). These results suggest that although mycobacterial CtpJs are involved in controlling $Co^{2+}$ levels they also participate

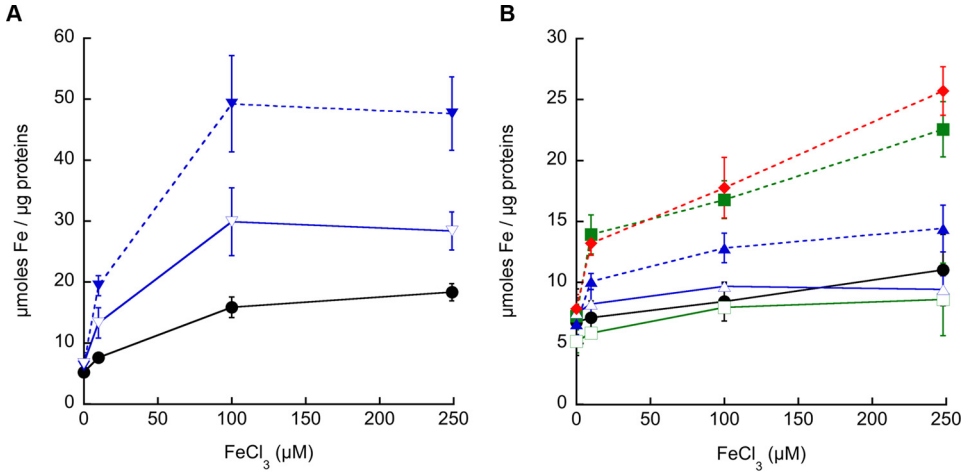


FIGURE 2. **Iron levels in mycobacterial $P_{1B4}$-ATPase mutant strains.** *A*, *M. smegmatis* WT (●; *black*), Δ*ctpJ* (▼; *blue*), and complemented (▽; *blue*) strains grown in LIMM supplemented with increasing concentrations of $FeCl_3$ for 4 h. *B*, *M. tuberculosis* WT (●; *black*), Δ*ctpD* (■; *green*), Δ*ctpD* complemented (□; *green*), Δ*ctpJ* (▲; *blue*), Δ*ctpJ* complemented (△; *blue*), and Δ*ctpD*:Δ*ctpJ* (◆; *red*) strains grown in LIMM supplemented with increasing concentrations of $FeCl_3$ for 8 h. Data are the mean ± S.E. (*error bars*) of three independent experiments.

in $Fe^{2+}$ efflux, particularly when they are the only $P_{1B4}$-ATPase in the organism as in *M. smegmatis*. In contrast, MtCtpD appears to play a dominant role in maintaining the cytoplasmic $Fe^{2+}$ level in this organism.

*Distinct Biochemical Properties of Mycobacterial $P_{1B4}$-ATPase*—P-ATPases couple the transmembrane transport of their substrate to ATP hydrolysis following the Albers-Post E1/E2-like mechanism (23). Consequently, the metal dependence of ATPase activity provides a starting point to analyze substrate selectivity. Previous reports showed that MsCtpJ, MtCtpD, and MtCtpJ are differently activated by $Co^{2+}$, $Ni^{2+}$, and to a lesser extent $Zn^{2+}$ (15, 16). The activation of mycobacterial $P_{1B4}$-ATPases by $Fe^{2+/3+}$ was tested using purified proteins stabilized in lipid/detergent micelles. All three proteins were strongly activated by $Fe^{2+}$ and only minimally by $Fe^{3+}$ (Fig. 3). For comparison, activation by $Co^{2+}$, $Ni^{2+}$, and $Zn^{2+}$ at 0.1 and 1 mM concentrations is shown. MtCtpD $Fe^{2+}$-dependent activity was ~2-fold higher than those observed in MtCtpJ and MsCtpJ (Table 1 and Fig. 3*D*) and quite similar to that of *B. subtilis* PfeT (3.25 ± 0.21 μmol/mg/h) (13). MtCtpD also showed significant activation at 1 mM $Zn^{2+}$ (Fig. 3*B*). $Zn^{2+}$ binding to $P_{1B4}$-ATPases as well as $Zn^{2+}$ transport has been reported (15, 30). The $K_{1/2}$ for $Fe^{2+}$ activation of the mycobacterial enzymes confirmed a tendency observed in *B. subtilis* PfeT: the larger activation by $Fe^{2+}$ is associated with a $K_{1/2}$ much larger than that of $Co^{2+}$ (Table 1). However, the observed $K_{1/2}$ values do not describe the selectivity to the enzymes. These parameters result from the $k_{on}/k_{off}$ of the metals binding the cytoplasmic facing transmembrane sites and the $k_{on}/k_{off}$ for the release/backward binding of the metal to the periplasmic facing sites (41). As shown below, equilibrium binding determinations of $K_D$ better report the relative selectivity for the activating metals.

The described $Fe^{2+}$-ATPase activities require the binding of the transported substrate to the TM-MBS. The stoichiometry of this interaction was verified by measuring $Fe^{2+}$ binding to MsCtpJ, MtCtpD, and MtCtpJ in non-turnover conditions lacking ATP (Table 1). The $His_6$-less enzymes were incubated with excess $Fe^{2+}$, unbound metal was removed by filtration, and bound metal was quantified by AAS. As expected, the proteins bind $Fe^{2+}$ in a 1:1 molar ratio. Discarding the possibility of nonspecific interactions, metal binding was largely abolished in the presence of 1.5 mM vanadate (not shown). This binding stoichiometry is similar to that previously observed for $Zn^{2+}$, $Ni^{2+}$, and $Co^{2+}$ binding to $P_{1B4}$-ATPases (15, 17). Notably, although the TM-MBSs of these enzymes appear to accommodate divalent cations, no significant binding of $Fe^{3+}$ was observed (not shown).

Mycobacterial $P_{1B4}$-ATPase affinities for $Fe^{2+}$ and $Co^{2+}$ under equilibrium conditions were determined by titration of isolated enzymes in the presence of the fluorescence indicator mag-fura-2 (15, 42). In these experiments, mag-fura-2 forms 1:1 indicator-metal complexes of known $K_D$. The concentration of free indicator can be spectrophotometrically monitored, and the free metal and metal-protein complex levels can be calculated. The enzyme-metal $K_D$ and the apparent stoichiometry of the interactions were obtained by fitting mag-fura-2 $A_{366}$ *versus* free metal concentration curves (Table 1). MsCtpJ and MtCtpJ showed a similar $K_D$ for $Fe^{2+}$. These were also comparable with those previously reported for $Co^{2+}$ (included in Table 1 for comparison). Notably, MtCtpD has ~3-fold higher affinity for $Fe^{2+}$ compared with $Co^{2+}$. Moreover, the affinity of MtCtpD is 20 times higher for $Fe^{2+}$ (lower $K_D$) and 5 times higher for $Co^{2+}$ when compared with those observed in the CtpJ enzymes. The relative preference of MtCtpD for $Fe^{2+}$ when compared with MtCtpJ further supports a dominant role of MtCtpD in $Fe^{2+}$ tolerance (Fig. 1).

*Distinct $Co^{2+}$ and $Fe^{2+}$ Coordination by MtCtpD*—Full appreciation of the different enzymatic activities and metal selectivity observed in $P_{1B4}$-ATPases requires understanding of the structural basis of these phenomena. $P_{1B4}$-ATPases share a number of invariant residues in the transmembrane region proposed to participate in metal coordination (19, 24–26). A six-coordinate $Co^{2+}$ species by the *Sulfitobacter* sp. $P_{1B4}$-ATPase has been postulated with participation of a Ser in the conserved SPC in the fourth TM and invariant His, Glu, and Thr in the

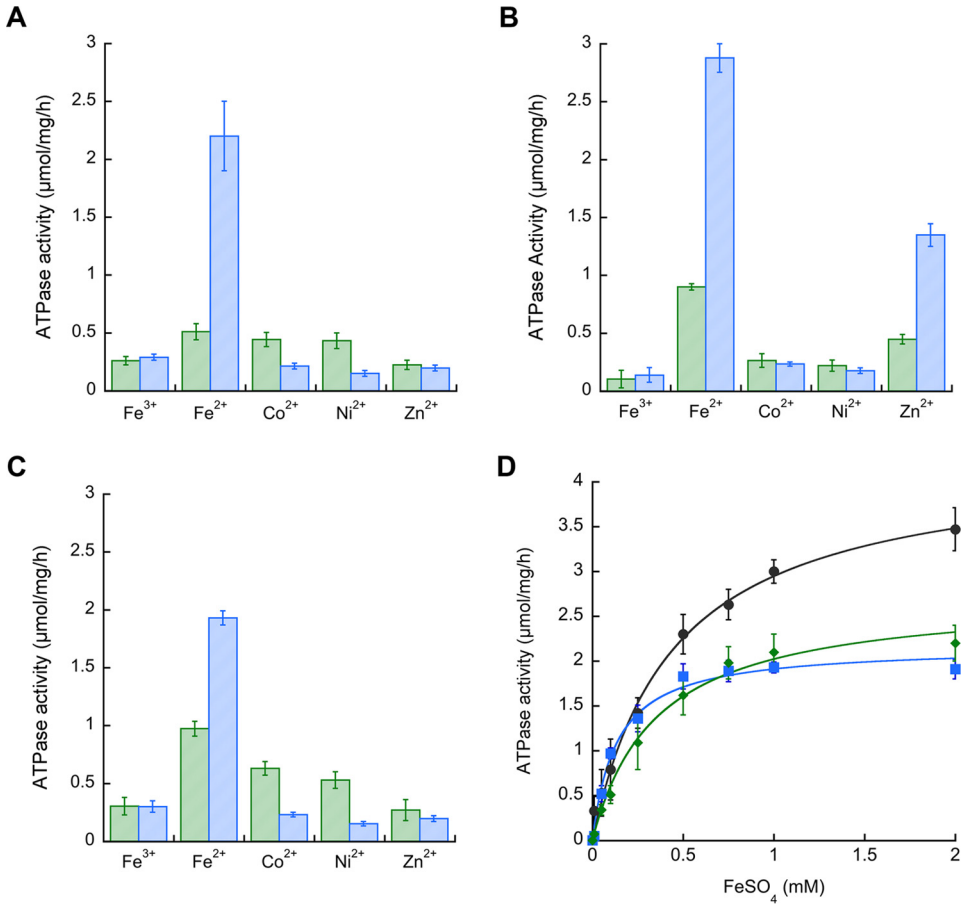


FIGURE 3. **Activation of mycobacterial $P_{1B4}$-ATPases by $Fe^{2+}$.** ATPase activity of purified MsCtpJ (*A*), MtCtpD (*B*), and MtCtpJ (*C*) in the presence of a 0.1 (*green bars*) or 1.0 mM (*blue bars*) concentration of the indicated metal ions was determined. *D*, $Fe^{2+}$ dependence of MsCtpJ (■; *blue*), MtCtpD (●; *black*), and MtCtpJ (◆; *green*) ATPase activities. Data are the mean ± S.E. (*error bars*) of three independent experiments performed in duplicate.

**TABLE 1**
**Summary of kinetic parameters, metal binding stoichiometry, and affinity of mycobacterial $P_{1B4}$-ATPases**

| | *M. smegmatis* CtpJ | | *M. tuberculosis* CtpD | | *M. tuberculosis* CtpJ | |
|---|---|---|---|---|---|---|
| | $Fe^{2+}$ | $Co^{2+}$ | $Fe^{2+}$ | $Co^{2+}$ | $Fe^{2+}$ | $Co^{2+}$ |
| **ATPase activity**[a] | | | | | | |
| $V_{max}$ (μmol/mg/h) | 2.73 ± 0.12 | 0.62 ± 0.03[b] | 4.25 ± 0.19 | 0.35 ± 0.03[b] | 2.16 ± 0.07 | 1.38 ± 0.12[b] |
| $K_{1/2}$ (μM) | 350 ± 45 | 4.1 ± 0.9[b] | 443 ± 54 | 4.8 ± 1.4[b] | 143 ± 18 | 6.3 ± 2.2[b] |
| **Metal stoichiometry**[c] | 1.0 ± 0.1 | 0.9 ± 0.1[b] | 1.1 ± 0.1 | 1.1 ± 0.1[b] | 1.1 ± 0.1 | 1.1 ± 0.3[b] |
| **Metal binding affinity**[d] | | | | | | |
| $K_D$ (μM) | 2.24 ± 0.43 | 2.59 ± 0.32[b] | 0.12 ± 0.04 | 0.33 ± 0.04 | 2.41 ± 0.27 | 1.60 ± 0.16 |
| $N$ | 1.44 ± 0.17 | 1.39 ± 0.22[b] | 1.32 ± 0.11 | 1.26 ± 0.04 | 1.35 ± 0.06 | 1.38 ± 0.05 |

[a] Values are the best fit parameters of activity *versus* $Fe^{2+}$ curves. Errors are asymptotic errors provided by the fitting software (Fig. 3*D*).
[b] Values were previously reported (15, 16).
[c] Values are the mean ± S.E. ($n = 3$).
[d] Values obtained by competitive metal binding with mag-fura-2. Values are the mean ± S.D. ($n = 3$).

sixth TM (17). Surprisingly, this coordination did not include the invariant Cys located in the fourth transmembrane segment of all $P_{1B}$-ATPases.

Considering the results shown above and the possible distinct $Fe^{2+}/Co^{2+}$ coordination, the binding environment of $Fe^{2+}$ and $Co^{2+}$ in MtCtpD was analyzed by XAS. The x-ray absorption near edge spectroscopy (XANES) portion of the XAS spectrum is element-specific and local bonding-sensitive; therefore it is useful for reporting the oxidation and coordination states of metals bound to the enzyme. The spectra of $Fe^{2+}$-loaded protein were compared with $Fe^{2+}$ and $Fe^{3+}$ model systems (Fig. 4*A*). The first inflection point energy for protein-bound iron occurs at 7127.6 eV, consistent with a 50%/50% $Fe^{2+}/Fe^{3+}$ redox state mixture. Although all spectra were closely screened for photoreduction, iron oxidation during protein concentration postmetal loading may have led to this observation. Pre-edge features observed in the XANES of iron-MtCtpD are characteristic of $1s \rightarrow 3d$ electronic transitions. These pre-edge features are consistent with pseudosymmetric six-coordinate iron-ligand systems (43). Cobalt-MtCtpD XANES pre-edge features and the general edge structure are consistent with $Co^{2+}$ bound to protein systems in a six-coordinate ligand environment as observed previously (Fig. 4*B*) (17, 44). The EXAFS region of an XAS spectrum provides high res-

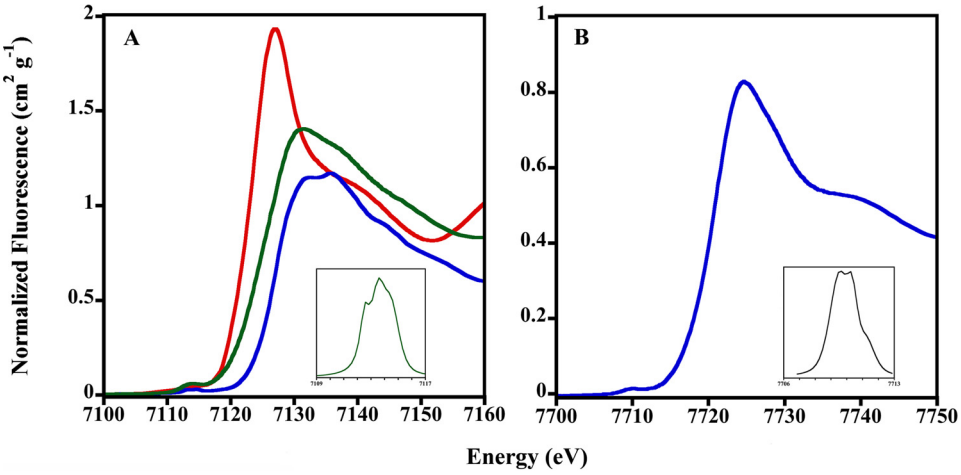


FIGURE 4. **Normalized iron and cobalt XANES spectra of MtCtpD.** *A*, XANES plot for iron-MtCtpD (*green*), $FeSO_4$ (*red*), and $Fe_2(SO_4)_3$ (*blue*). Peak maximum, 7113.5 eV; total peak area, 7.91. *B*, XANES plot for cobalt-MtCtpD (*blue*). Peak maximum, 7709.6 eV; total peak area, 1.92. *Insets* show expansion of spline-subtracted pre-edge feature for the $1s \rightarrow 3d$ transition for each element.

olution distances for ligand coordination environments of metals bound to metalloproteins. Fourier transform of the EXAFS provides a pseudoradial distribution function of ligand environments surrounding the metal. EXAFS analysis was used to compare differences in coordination of iron and cobalt to MtCtpD (Fig. 5). The resulting coordination number, ligand identity, bond lengths, and statistical fitting parameters are described in Table 2. The iron-MtCtpD spectrum was best simulated by a ligand environment containing five oxygen/nitrogen ligands at two sets of coordinating distances. Long range iron-ligand scattering was best fit with four Fe–C ligands. The general features in the iron EXAFS and bond lengths obtained from the simulations suggest that iron is most likely coordinated by six oxygen/nitrogen-based side chain ligands from amino acids and water molecules. The cobalt-MtCtpD EXAFS served as a comparison for the iron bound to MtCtpD. The best fit simulation contained two unique Co–O/N environments (Table 2). The Co–O/N bond lengths, compared with crystallographically characterized model compounds in the Cambridge Structural Database, are again consistent with five- to six-coordinate Co–$(O/N)_6$ compounds (45). This is similar to what has been observed in the *Sulfitobacter* sp. $P_{1B4}$-ATPase (17).

The spectroscopy analysis points to a distinct coordination for $Co^{2+}$ and $Fe^{2+}$. However, the spectroscopy is not able to reveal alternative ligands. Conserved residues of MtCtpD possibly involved in metal coordination are Ser-316 and Cys-318 in TM4 and His-642, Glu-643, Gly-644, Ser-645, and Thr-646 in TM6. Seeking a more detailed understanding of the $Fe^{2+}$ and $Co^{2+}$ coordination at the TM-MBS, residues likely involved in the metal coordination were exchanged by site-directed mutagenesis, and the resulting proteins were functionally characterized. The single mutants E643D and T646S (included as conservative control modifications) and G644A and S645A did not alter the $Co^{2+}$- or $Fe^{2+}$-ATPase activities of MtCtpD (Fig. 6). In agreement with previous reports, mutation of S316A, H642A, E643A, or T646A led to significant loss of $Co^{2+}$ ATPase activity (17). The single substitutions S316A, E643A, and T646A equally affected the $Co^{2+}$- and $Fe^{2+}$-ATPase activities. However, the H642A mutation largely abolished $Co^{2+}$ stimulation (6% of WT activity) while preserving significant $Fe^{2+}$ sensitivity (33%) at saturating metal concentrations. In contrast, the C318A mutation had diminished $Fe^{2+}$ activation (18%) while retaining 39% of the $Co^{2+}$-ATPase activity. The differential effects of H642A and C318A mutations on the ATPase activity point toward a plausible mechanism. It appears that CtpD differentiates $Co^{2+}$ and $Fe^{2+}$ as substrates perhaps via alternative coordination despite binding these ions with quite similar affinities.

Considering that the ATPase activities might be affected by the removal of a ligating group or by the inability to undergo structural changes required for transport, the capability of the C318A and H642A mutant proteins to bind $Co^{2+}$ and $Fe^{2+}$ was tested. In comparison, the C318A mutant showed significantly lowered MtCtpD affinity for $Fe^{2+}$, but it did not change the binding affinity for $Co^{2+}$, suggesting an important role of this conserved Cys in $Fe^{2+}$ binding (Fig. 7 and Table 3). The critical role of Cys-318 was further confirmed by the determination of the metal binding by AAS after incubation of the C318A mutant protein with metals at concentrations 10 times over the observed $K_D$. The C318A mutant protein was able to bind $1.05 \pm 0.14$ $Co^{2+}$ but only $0.32 \pm 0.06$ $Fe^{2+}$. Finally, the H642A mutant had no detectable effect on $Fe^{2+}$ or $Co^{2+}$ binding affinities compared with WT (Table 3), raising the possibility that His-642 has a role other than the direct participation in the TM-MBS.

## Discussion

The substrates and consequent functional roles of bacterial and eukaryotic $P_{1B4}$-ATPases have remained elusive as their capabilities to transport different transition metals have been reported (15–17, 28–30). This is relevant as some of these transporters are required for bacterial virulence (16, 18) and critical for metal homeostasis in chloroplasts (29, 46). An extra layer of complexity is present in bacterial systems containing homologous non-redundant $P_{1B4}$-ATPases (16). From a different perspective, defining $P_{1B4}$-ATPases substrates is significant to understanding the coordination of transition metals by

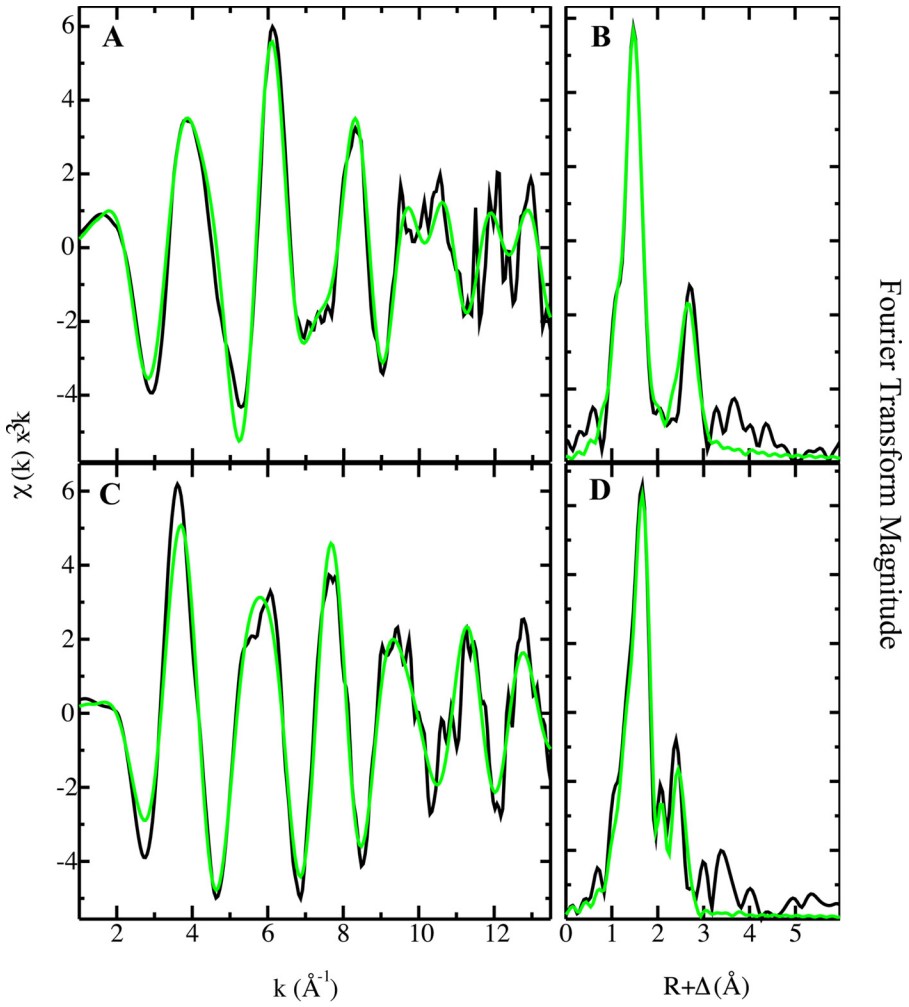


FIGURE 5. **Iron and cobalt EXAFS and Fourier transform with best fit simulations.** Iron-MtCtpD raw $k^3$-weighted EXAFS (*A*) and phase-shifted Fourier transform (*B*) are shown. Cobalt-MtCtpD raw $k^3$-weighted EXAFS (*C*) and phase-shifted Fourier transform (*D*) are shown. Raw unfiltered data are shown in *black*, and best fit simulations are shown in *green*.

**TABLE 2**

**Summary of the iron and cobalt EXAFS simulations for metals bound to MtCtpD**

Data utilized a *k* range of 1–13.5 $Å^{-1}$.

| Nearest neighbor ligand environment[a] | | | | | Long range ligand environment[a] | | | | |
|---|---|---|---|---|---|---|---|---|---|
| Metal | Atom[b] | $R^c$ | C.N.[d] | $\sigma^{2e}$ | Atom[b] | $R^c$ | C.N.[d] | $\sigma^{2e}$ | $F'^f$ |
| | | Å | | | | Å | | | |
| Iron | Oxygen/nitrogen | 1.93 | 2.5 | 1.93 | Carbon | 3.09 | 4.0 | 2.46 | 0.32 |
| | Oxygen/nitrogen | 2.07 | 2.5 | 2.41 | | | | | |
| Cobalt | Oxygen/nitrogen | 2.09 | 4.0 | 3.73 | Carbon | 2.91 | 4.0 | 4.43 | 0.33 |
| | Oxygen/nitrogen | 1.97 | 1.0 | 3.91 | | | | | |

[a] Independent metal-ligand scattering environment.
[b] Scattering atoms.
[c] Average metal-ligand bond length.
[d] Average metal-ligand coordination number.
[e] Average Debye-Waller factor (Å × $10^3$).
[f] Number of degrees of freedom weighted mean square deviation between data and fit.

transport proteins as well as likely additional selectivity mechanisms acting *in vivo*. Here we describe the roles of mycobacterial $P_{14B}$-ATPases in $Fe^{2+}$ homeostasis, the kinetics of transport, and the structural elements that in part determine the selectivity of these enzymes. These results indicate that mycobacterial $P_{14B}$-ATPases are $Fe^{2+}/Co^{2+}$-ATPases; however, the various isoforms show differential participation in the homeostasis of these ions.

*Mycobacterial $P_{1B4}$-ATPases Participates in Both $Fe^{2+}$ and $Co^{2+}$ Homeostasis*—We observed that mycobacterial CtpJ proteins contribute to the homeostasis of $Fe^{2+}$ and $Co^{2+}$ to different extents. *M. smegmatis* has a single $P_{1B4}$-ATPase, MsCtpJ. Expression of the coding gene is induced by $Co^{2+}$ and partially by the superoxide generator paraquat but not by $H_2O_2$ (15). Deletion of *MsctpJ* leads to lower tolerance to $Co^{2+}$, $Fe^{2+}$, and hemin as well as increments in intracellular $Co^{2+}$ and $Fe^{2+}$

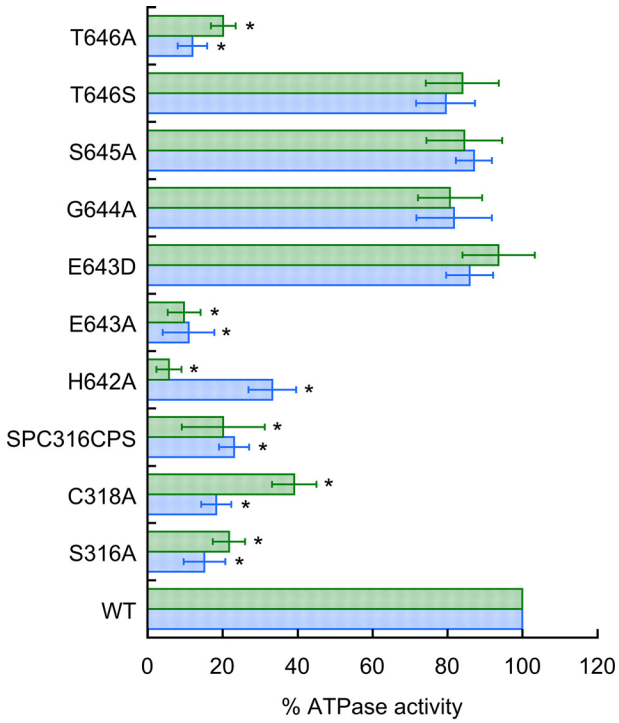


FIGURE 6. **ATPase activity of MtCtpD proteins carrying substitutions of residues likely participating in the metal binding site in the presence of 0.1 mM $Co^{2+}$ (*green bars*) or 1 mM $Fe^{2+}$ (*blue bars*).** Replacement SPC16CPS indicates the double mutant S316C/C318S. Activities were normalized to those of the wild type MtCtpD. Data are the mean ± S.E. (*error bars*) of three independent experiments performed in duplicate. Significant differences from the WT as determined by Student's *t* test are indicated (*, $p < 0.01$).

levels (Fig. 1) (15). The *M. tuberculosis* genome encodes two $P_{1B4}$-ATPases. MtCtpJ expression, like MsCtpJ, is induced by $Co^{2+}$ and to a lesser extent by redox stressors and $Fe^{2+}$ (16). The *MtΔctpJ* strain accumulates higher levels of both $Co^{2+}$ and $Fe^{2+}$ (Fig. 1) (16), again in a fashion similar to that of the *MsΔctpJ* strain. These characteristics appear similar to those observed for PfteT, the single $P_{1B4}$-ATPase present in *B. subtilis* (13). The comparable functions suggested by the observed phenotypes correlate with the analogous biochemistry of MsCtpJ, MtCtpJ, and *B. subtilis* PfteT. These three ATPases transport $Fe^{2+}$ and $Co^{2+}$ with surprisingly similar $V_{max}$ and $K_{1/2}$ for activation. Moreover, both CtpJs bind $Fe^{2+}$ and $Co^{2+}$ with micromolar affinities (equilibrium binding determinations have not been performed for PfeT). These affinities explain the observed capability of these enzymes to influence the cellular response to STN when extracellular iron is maintained at just 10 μM. More importantly, 2–3 μM $Fe^{2+}$ affinities appear consistent with reported free $Fe^{2+}$ levels in the 1–10 μM region (4). In fact, the iron-sensing transcriptional regulators Fur and IdeR have 9 μM $K_D$ for $Fe^{2+}$ (47, 48), indicating that these regulators are sensitive to the same concentration of $Fe^{2+}$ as the $P_{1B4}$-ATPases. Consequently, efflux CtpJ ATPases and influx transporter regulators are likely to coordinately respond to changes in metal levels not only under $Fe^{2+}$ stress conditions but also under normal conditions.

*Homologous $P_{1B4}$-ATPases Present in Mycobacterial Genomes Have Distinct Roles—M. tuberculosis*, as in other mycobacteria, has an additional $P_{1B4}$-ATPase, CtpD. Notably, MtCtpD, but not MtCtpJ, is required for bacterial virulence. What unique function does CtpD provide? The *MtΔctpD* strain is more sensitive to iron stress and accumulates higher levels of this metal than *MtΔctpJ*. The phenotypic differences between the *MtΔctpD* and *MtΔctpJ* strains should have a molecular basis either in the biochemistry of these enzymes or the iron pool that they transport. Notably, the phenotype of the *MtΔctpD*:*ΔctpJ* double mutant strain is similar to that of the *MtΔctpD* cells, suggesting that CtpD and CtpJ use the same iron pool as a substrate, and this can be controlled by MtCtpD alone. Alternatively, the molecular activities of MtCtpD and MtCtpJ appear distinct. MtCtpD has significantly higher $Fe^{2+}$-ATPase activity. Moreover, if the relative activation induced by $Fe^{2+}/Co^{2+}$ is considered, MtCtpD shows $Fe^{2+}$ activity 12 times larger than that generated by $Co^{2+}$. On the contrary, MtCtpJ shows higher activation by $Co^{2+}$ than MtCtpD and only a 1.5 $Fe^{2+}$-ATPase:$Co^{2+}$-ATPase ratio. Although these relative activities approximately correlate with the observed phenotypes, the higher affinity of MtCtpD for $Fe^{2+}$ ($K_D$ of 0.1 μM) appears to confer its dominant role in $Fe^{2+}$ homeostasis. This $K_D$ is 1 order of magnitude smaller than that reported for $Fe^{2+}$-sensing transcriptional regulators of influx systems (47, 48). Distinct from CtpJ, CtpD is not induced by divalent metals but by redox stressors, such as the nitric oxide generator nitroprusside and the respiratory poison cyanide (16). In fact, the region upstream of *ctpD* contains the TTG *XXXX*TTC*XXG* operator sequence for the redox-sensing MtFurA regulator (49). Considering the release of $Fe^{2+}$ from iron-sulfur and mononuclear iron-containing proteins upon redox stress, it can be hypothesized that CtpD constitutes an early response to $Fe^{2+}$ dyshomeostasis that is independent of efflux (CtpJ), storage (bacterioferritin), and regulators (IdeR) that respond to higher free $Fe^{2+}$ levels.

*The Coordination of $Fe^{2+}$ by $P_{1B4}$-ATPases Likely Requires the Invariant Cys in the Fourth TM*—Metal selectivity is central to the physiological roles of $P_{1B}$-ATPases. In early studies, invariant Cys in the sixth TM (fourth TM in $P_{1B4}$-ATPases) were instrumental in defining $P_{1B}$-ATPases. Detection of other conserve residues in the transmembrane region led to the identification of $P_{1B}$-ATPases subgroups (19). The participation of these signature residues in the binding sites of $P_{1B1}$ $Cu^+$-ATPases and $P_{1B2}$ $Zn^{2+}$-ATPases was later established (25, 26). Then it was relevant to establish the metal coordination in $P_{1B4}$-ATPases. Previous studies proposed that $P_{1B4}$-ATPases coordinate $Co^{2+}$ with a Ser in the conserved SPC in the fourth TM and invariant His, Glu, and Thr in the sixth TM of these proteins (17). Surprisingly, no participation of the archetypical Cys in the fourth TM in $Co^{2+}$ coordination was observed. However, a different coordination of $Fe^{2+}$ by MtCtpD might explain its distinct biochemistry, *i.e.* higher affinity for $Fe^{2+}$ and $Co^{2+}$ and higher activity in the presence of $Fe^{2+}$. We studied the coordination of $Fe^{2+}$ and $Co^{2+}$ while bound to MtCtpD TM-MBS by XAS and functionally analyzed variants carrying mutations in putative coordinating groups. XAS data indicate that both $Fe^{2+}$ and $Co^{2+}$ are coordinated by five to six oxygen/nitrogen ligands in a manner similar to that described previously for the *Sulfitobacter* sp. $P_{1B4}$-ATPase. That is, the spectroscopy does not

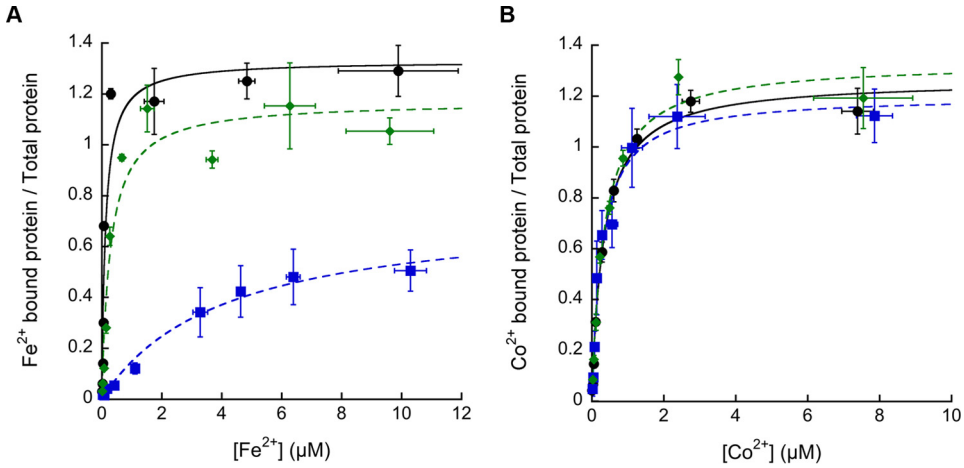


FIGURE 7. **$Fe^{2+}$ and $Co^{2+}$ binding affinities to MtCtpD WT, C318A, and H642A protein variants.** Dissociation constants of MtCtpD WT (●; *black*), C318A (■; *blue*), and H642A (◆; *green*) for $Fe^{2+}$ (*A*) and $Co^{2+}$ (*B*) were determined. The data were fit to $v = n[Me^{2+}_{free}]/K_D(1 + ([Me^{2+}_{free}]/K_D)$ using values shown in Table 3. Data are the mean ± S.D. (*error bars*) of three independent experiments.

**TABLE 3**
**Comparison of $Fe^{2+}$ and $Co^{2+}$ dissociation constants of MtCtpD and C318A and H642A variants**

| MtCtpD | $Fe^{2+}$ | | $Co^{2+}$ | |
|---|---|---|---|---|
| | $K_D$[a] | $n$[a] | $K_D$ | $n$ |
| | μM | | μM | |
| WT | 0.12 ± 0.04 | 1.32 ± 0.11 | 0.33 ± 0.04 | 1.26 ± 0.04 |
| C318A | 4.01 ± 0.89 | 0.74 ± 0.07 | 0.28 ± 0.08 | 1.20 ± 0.05 |
| H642A | 0.28 ± 0.08 | 1.14 ± 0.10 | 0.34 ± 0.05 | 1.33 ± 0.14 |

[a] Values obtained by fitting curves resulting from competitive metal binding with mag-fura-2 (Fig. 7). Values are the mean ± S.D. ($n$ = 3).

show the participation of sulfur atoms from the invariant Cys in the fourth TM as a metal ligand.

Notably, mutagenesis studies showed an alternative portrait of MtCtpD TM-MBS. As shown in the case the *Sulfitobacter* sp. $P_{1B4}$-ATPase, we observed that mutation of S316A, H642A, E643A, and T646A led to an almost complete inhibition of $Co^{2+}$ activation, whereas replacement C318A retains significant (39%) $Co^{2+}$-ATPase activity. A different pattern is observed, however, for the effects of these mutations on the $Fe^{2+}$-ATPase. In this case, H642A retains some activity, whereas C318A causes a larger decrease in the activation by $Fe^{2+}$. Although these differences are not dramatic, they suggest a putative differential involvement of these residues. Determination of the equilibrium binding affinities provided a more detailed view. Surprisingly, mutation H642A did not affect the metal binding to MtCtpD, suggesting that the reduced $V_{max}$ of this mutant is associated with alterations in rate-limiting conformational steps rather than ion coordination. Keep in mind that metal release is the rate-limiting step in P-type ATPases (21, 50). More remarkably, replacement of C318A leads to a large reduction in the affinity for $Fe^{2+}$ without affecting $Co^{2+}$ binding. This datum in itself does not show a role of the conserved Cys in coordinating metals but suggests a direct effect, perhaps steric or through the second coordination sphere, in determining the affinity for $Fe^{2+}$. In this case, the conservation of this Cys in the CPS signature sequence appears to be a logical consequence of the need to maintain a high binding affinity for $Fe^{2+}$.

In summary, our observations suggest that mycobacterial $P_{1B4}$-ATPases play a central role in $Fe^{2+}$ homeostasis. CtpD in particular, likely regulated by FurA, constitutes part of the cellular response to redox-induced damage of iron centers.

*Author Contributions*—S. J. P. conducted most of the experiments, analyzed the results, and wrote the initial draft of the manuscript. B. E. L. performed X-ray spectroscopy analysis. J. E. L. and S. N. conducted growth and metal tolerance experiments using *M. tuberculosis* strains. C. M. S. oversaw *in vivo* experiments with *M. tuberculosis* and participated in manuscript revision. T. L. S. supervised x-ray spectroscopic analysis and participated in manuscript revision. J. M. A. conceived the idea for the project, directed the project, and wrote the paper with S. J. P.

*Acknowledgments—We thank Andrew Baez (Worcester Polytechnic Institute) for assistance with early experiments. X-ray absorption spectroscopic studies were performed at the Stanford Synchrotron Radiation Lightsource (SSRL). SSRL is a national user facility operated by Stanford University on behalf of the United States Department of Energy, Office of Basic Energy Sciences. The SSRL Structural Molecular Biology Program is supported by the Department of Energy, Office of Biological and Environmental Research, and by the National Institutes of Health, National Center for Research Resources, Biomedical Technology Program.*

## References

1. Fraústo da Silva, J. J. R., and Williams, R. J. P. (2001) *The Biological Chemistry of the Elements: the Inorganic Chemistry of Life*, 2nd Ed., Oxford University Press, Oxford
2. Andrews, S. C., Robinson, A. K., and Rodríguez-Quiñones, F. (2003) Bacterial iron homeostasis. *FEMS Microbiol. Rev.* **27,** 215–237
3. Anjem, A., and Imlay, J. A. (2012) Mononuclear iron enzymes are primary targets of hydrogen peroxide stress. *J. Biol. Chem.* **287,** 15544–15556
4. Keyer, K., and Imlay, J. A. (1996) Superoxide accelerates DNA damage by elevating free-iron levels. *Proc. Natl. Acad. Sci. U.S.A.* **93,** 13635–13640
5. Jang, S., and Imlay, J. A. (2007) Micromolar intracellular hydrogen peroxide disrupts metabolism by damaging iron-sulfur enzymes. *J. Biol. Chem.* **282,** 929–937
6. Varghese, S., Wu, A., Park, S., Imlay, K. R., and Imlay, J. A. (2007) Submicromolar hydrogen peroxide disrupts the ability of Fur protein to control free-iron levels in *Escherichia coli*. *Mol. Microbiol.* **64,** 822–830
7. Rodriguez, G. M. (2006) Control of iron metabolism in *Mycobacterium tuberculosis*. *Trends Microbiol.* **14,** 320–327
8. Lucarelli, D., Vasil, M. L., Meyer-Klaucke, W., and Pohl, E. (2008) The

metal-dependent regulators FurA and FurB from *Mycobacterium tuberculosis*. *Int. J. Mol. Sci.* **9,** 1548–1560
9. Pandey, R., and Rodriguez, G. M. (2014) IdeR is required for iron homeostasis and virulence in *Mycobacterium tuberculosis*. *Mol. Microbiol.* **91,** 98–109
10. Grass, G., Otto, M., Fricke, B., Haney, C. J., Rensing, C., Nies, D. H., and Munkelt, D. (2005) FieF (YiiP) from *Escherichia coli* mediates decreased cellular accumulation of iron and relieves iron stress. *Arch. Microbiol.* **183,** 9–18
11. Bennett, B. D., Brutinel, E. D., and Gralnick, J. A. (2015) A ferrous iron exporter mediates iron resistance in *Shewanella oneidensis* MR-1. *Appl. Environ. Microbiol.* **81,** 7938–7944
12. Frawley, E. R., and Fang, F. C. (2014) The ins and outs of bacterial iron metabolism. *Mol. Microbiol.* **93,** 609–616
13. Guan, G., Pinochet-Barros, A., Gaballa, A., Patel, S. J., Argüello, J. M., and Helmann, J. D. (2015) PfeT, a $P_{1B4}$-type ATPase, effluxes ferrous iron and protects *Bacillus subtilis* against iron intoxication. *Mol. Microbiol.* **98,** 787–803
14. Gaballa, A., and Helmann, J. D. (2002) A peroxide-induced zinc uptake system plays an important role in protection against oxidative stress in *Bacillus subtilis*. *Mol. Microbiol.* **45,** 997–1005
15. Raimunda, D., Long, J. E., Sassetti, C. M., and Argüello, J. M. (2012) Role in metal homeostasis of ctpd, a $Co^{2+}$ transporting $P_{1B4}$-ATPase of *Mycobacterium smegmatis*. *Mol. Microbiol.* **84,** 1139–1149
16. Raimunda, D., Long, J. E., Padilla-Benavides, T., Sassetti, C. M., and Argüello, J. M. (2014) Differential roles for the $Co^{2+}$/$Ni^{2+}$ transporting ATPases, CtpD and CtpJ, in *Mycobacterium tuberculosis* virulence. *Mol. Microbiol.* **91,** 185–197
17. Zielazinski, E. L., Cutsail, G. E., 3rd, Hoffman, B. M., Stemmler, T. L., and Rosenzweig, A. C. (2012) Characterization of a cobalt-specific $P_{1B}$-ATPase. *Biochemistry* **51,** 7891–7900
18. McLaughlin, H. P., Xiao, Q., Rea, R. B., Pi, H., Casey, P. G., Darby, T., Charbit, A., Sleator, R. D., Joyce, S. A., Cowart, R. E., Hill, C., Klebba, P. E., and Gahan, C. G. (2012) A putative P-type ATPase required for virulence and resistance to haem toxicity in *Listeria monocytogenes*. *PLoS One* **7,** e30928
19. Argüello, J. M. (2003) Identification of ion selectivity determinants in heavy metal transport $P_{1B}$-type ATPases. *J. Membr. Biol.* **195,** 93–108
20. Smith, A. T., Barupala, D., Stemmler, T. L., and Rosenzweig, A. C. (2015) A new metal binding domain involved in cadmium, cobalt and zinc transport. *Nat. Chem. Biol.* **11,** 678–684
21. Argüello, J. M., Eren, E., and González-Guerrero, M. (2007) The structure and function of heavy metal transport $P_{1B}$-ATPases. *Biometals* **20,** 233–248
22. Rosenzweig, A. C., and Argüello, J. M. (2012) Toward a molecular understanding of metal transport by $P_{1B}$-type ATPases. *Curr. Top. Membr.* **69,** 113–136
23. Argüello, J. M., González-Guerrero, M., and Raimunda, D. (2011) Bacterial transition metal $P_{1B}$-ATPases: transport mechanism and roles in virulence. *Biochemistry* **50,** 9940–9949
24. Padilla-Benavides, T., Long, J. E., Raimunda, D., Sassetti, C. M., and Argüello, J. M. (2013) A novel $P_{1B}$-type $Mn^{2+}$-transporting ATPase is required for secreted protein metallation in mycobacteria. *J. Biol. Chem.* **288,** 11334–11347
25. Raimunda, D., Subramanian, P., Stemmler, T., and Argüello, J. M. (2012) A tetrahedral coordination of zinc during transmembrane transport by P-type $Zn^{2+}$-ATPases. *Biochim. Biophys. Acta* **1818,** 1374–1377
26. González-Guerrero, M., Eren, E., Rawat, S., Stemmler, T. L., and Argüello, J. M. (2008) $Cu^{+}$ transporting ATPases: structure of the two transmembrane $Cu^{+}$ transport sites. *J. Biol. Chem.* **283,** 29753–29759
27. Argüello, J. M., Raimunda, D., and González-Guerrero, M. (2012) Metal transport across biomembranes: emerging models for a distinct chemistry. *J. Biol. Chem.* **287,** 13510–13517
28. Moreno, I., Norambuena, L., Maturana, D., Toro, M., Vergara, C., Orellana, A., Zurita-Silva, A., and Ordenes, V. R. (2008) AtHMA1 is a thapsigargin-sensitive $Ca^{2+}$/heavy metal pump. *J. Biol. Chem.* **283,** 9633–9641
29. Seigneurin-Berny, D., Gravot, A., Auroy, P., Mazard, C., Kraut, A., Finazzi, G., Grunwald, D., Rappaport, F., Vavasseur, A., Joyard, J., Richaud, P., and Rolland, N. (2006) HMA1, a new cu-ATPase of the chloroplast envelope, is essential for growth under adverse light conditions. *J. Biol. Chem.* **281,** 2882–2892
30. Scherer, J., and Nies, D. H. (2009) CzcP is a novel efflux system contributing to transition metal resistance in *Cupriavidus metallidurans* CH34. *Mol. Microbiol.* **73,** 601–621
31. Rodriguez, G. M., and Smith, I. (2006) Identification of an ABC transporter required for iron acquisition and virulence in *Mycobacterium tuberculosis*. *J. Bacteriol.* **188,** 424–430
32. Bradford, M. M. (1976) A rapid and sensitive method for the quantitation of microgram quantities of protein utilizing the principle of protein-dye binding. *Anal. Biochem.* **72,** 248–254
33. Studier, F. W. (2005) Protein production by auto-induction in high density shaking cultures. *Protein Expr. Purif.* **41,** 207–234
34. Mandal, A. K., Cheung, W. D., and Argüello, J. M. (2002) Characterization of a thermophilic P-type $Ag^{+}$/$Cu^{+}$-ATPase from the extremophile *Archaeglobus fulgidus*. *J. Biol. Chem.* **277,** 7201–7208
35. Rosadini, C. V., Gawronski, J. D., Raimunda, D., Argüello, J. M., and Akerley, B. J. (2011) A novel zinc binding system, ZevAB, is critical for survival of nontypeable *Haemophilus influenzae* in a murine lung infection model. *Infect. Immun.* **79,** 3366–3376
36. Eren, E., Kennedy, D. C., Maroney, M. J., and Argüello, J. M. (2006) A novel regulatory metal binding domain is present in the C terminus of *Arabidopsis* $Zn^{2+}$-ATPase HMA2. *J. Biol. Chem.* **281,** 33881–33891
37. Guo, J., Giedroc, D.P. (1997) Zinc site redesign in t4 gene 32 protein: structure and stability of Co(II) complexes formed by wild-type and metal ligand substitution mutants. *Biochemistry* **36,** 730–742
38. Lanzetta, P. A., Alvarez, L. J., Reinach, P. S., and Candia, O. A. (1979) An improved assay for nanomole amounts of inorganic phosphate. *Anal. Biochem.* **100,** 95–97
39. George, G., and Pickering, I. (1995) *EXAFSPAK: a Suite of Computer Programs for Analysis of X-ray Absorption Spectra*, Stanford Synchrotron Radiation Lightsource, Menlo Park, CA
40. Yeowell, H. N., and White, J. R. (1982) Iron requirement in the bactericidal mechanism of streptonigrin. *Antimicrob. Agents Chemother.* **22,** 961–968
41. Segel, I. H. (1993) *Enzyme Kinetics*, pp. 534–543, John Wiley and Sons, Inc., New York
42. Eren, E., González-Guerrero, M., Kaufman, B. M., and Argüello, J. M. (2007) Novel $Zn^{2+}$ coordination by the regulatory N-terminus metal binding domain is present of *Arabidopsis thaliana* $Zn^{2+}$-ATPase HMA2. *Biochemistry* **46,** 7754–7764
43. Westre, T. E., Kennepohl, P., DeWitt, J. G., Hedman, B., Hodgson, K. O., and Solomon, E. I. (1997) A multiplet analysis of Fe k-edge 1s → 3d pre-edge features of iron complexes. *J. Am. Chem. Soc.* **119,** 6297–6314
44. Rhine, M. A., Rodrigues, A. V., Bieber Urbauer, R. J., Urbauer, J. L., Stemmler, T. L., and Harrop, T. C. (2014) Proton-induced reactivity of NO− from a $\{CoNO\}^8$ complex. *J. Am. Chem. Soc.* **136,** 12560–12563
45. Allen, F. H. (2002) The Cambridge Structural Database: a quarter of a million crystal structures and rising. *Acta Crystallogr. B* **58,** 380–388
46. Boutigny, S., Sautron, E., Finazzi, G., Rivasseau, C., Frelet-Barrand, A., Pilon, M., Rolland, N., and Seigneurin-Berny, D. (2014) HMA1 and PAA1, two chloroplast-envelope $P_{1B}$-ATPases, play distinct roles in chloroplast copper homeostasis. *J. Exp. Bot.* **65,** 1529–1540
47. Mills, S. A., and Marletta, M. A. (2005) Metal binding characteristics and role of iron oxidation in the ferric uptake regulator from *Escherichia coli*. *Biochemistry* **44,** 13553–13559
48. Chou, C. J., Wisedchaisri, G., Monfeli, R. R., Oram, D. M., Holmes, R. K., Hol, W. G., and Beeson, C. (2004) Functional studies of the *Mycobacterium tuberculosis* iron-dependent regulator. *J. Biol. Chem.* **279,** 53554–53561
49. Sala, C., Forti, F., Di Florio, E., Canneva, F., Milano, A., Riccardi, G., and Ghisotti, D. (2003) *Mycobacterium tuberculosis* FurA autoregulates its own expression. *J. Bacteriol.* **185,** 5357–5362
50. Heyse, S., Wuddel, I., Apell, H. J., and Stürmer, W. (1994) Partial reactions of the Na,K-ATPase: determination of rate constants. *J. Gen. Physiol.* **104,** 197–240